Numerical investigation of transverse sonic injection in a non-reacting supersonic combustor

P Manna and **D Chakraborty***
Defence Research and Development Laboratory, Kanchanbagh, Hyderabad, India

The manuscript was received on 25 November 2003 and was accepted after revision for publication on 11 May 2005.

DOI: 10.1243/095441005X30261

Abstract: Efficient combustion and heat release in scramjet flows depend on effective mixing of the fuel in supersonic streams. Usually, transverse sonic injection in-stages are employed as one of the suitable means for efficient supersonic combustor design. Numerical simulations are carried out to study the mixing characteristics of staged sonic air injections in supersonic stream ($M = 2.07$) behind a backward-facing step in scramjet combustor by solving three-dimensional Navier–Stokes equations along with K–ε turbulence model with a commercial CFD software CFX-TASCFlow. Computed results of the jet penetration and spreading show very good agreement with the experimental values and the results of other computations. A good overall match has been obtained between the experimental values and the computation for various flow profiles at various axial locations in the combustor. However, the values differ in the near-field region at the injection plane. The assumed uniformity of the flow-field properties at the injection orifice and/or the inadequacy of the turbulence model considered in this study is conjectured to be the cause of the difference.

Keywords: scramjet, transverse injection, backward facing step, dynamic pressure ratio

1 INTRODUCTION

A vital part of the effort to develop air-breathing propulsion systems capable of sustaining hypersonic flight in the atmosphere is the ability to understand the complex mixing and combustion process inside a scramjet combustor. For the scramjet propulsion device, where chemical reaction and heat release occur in a supersonic stream, adequate mixing of fuel and oxidizer is an essential requirement. Proper choice of the injection scheme plays a very important role in the efficient design of the scramjet combustor.

A combination of transverse and tangential injectors is generally employed in the scramjet combustor. The transverse injector is used predominantly at the lower Mach numbers as it provides good fuel penetration, mixing, and heat release but at the expense of a larger pressure loss. Tangential (in-stream) injection results in lower total pressure loss and less fuel penetration; therefore it must be accompanied by means of mixing enhancements. A backward-facing step and the staged injection are generally employed to create the region of recirculation for flame holding in the supersonic flow field and to avoid intake – combustor interactions. Staged sonic transverse injection in a supersonic stream has been investigated in this work.

Transverse injection of an underexpanded sonic or supersonic jet into a supersonic free stream produces several flow structures. The schematic of the field is shown in Fig. 1. The supersonic flow undergoes expansion at the corner of the base. As the free stream is blocked partially by the secondary flow, a strong bow shock wave is formed in front of the injection point followed by a barrel shock. Also ahead of the injection point, the boundary layer separates because of the interaction between shock waves and boundary layer. Downstream of the injection point, the boundary layer reattaches and a

*Corresponding author: Computational Combustion Dynamics Division, Directorate of Computational Dynamics, Defence Research and Development Laboratory, Kanchanbagh, Hyderabad, India.

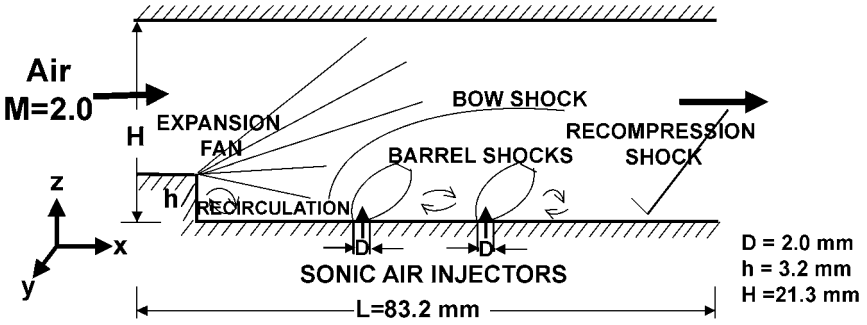

Fig. 1 Schematic of test set-up

recompression shock wave is generated. Hence, this flow field is quite complicated and various shock waves–boundary layer interactions exist in the whole region.

Many early investigations of the transverse gaseous jet in supersonic cross-flow revolved around qualitative examinations of the underexpanded injection flow field and analytical description of the injectant penetration depth as a function of various flow parameters [**1**, **2**]. Hersch *et al.* [**3**] measured the penetration of helium jet into Mach 2 stream over a flat plate from Schlieren photographs through densitometer analysis. Papamoschou *et al.* [**4**] investigated the effect of free stream Mach number, jet Mach number, static pressure ratio, density ratio, and momentum ratio on penetration using Schlieren photography. Results indicated that jet penetration into a supersonic cross-flow was principally dependent on the momentum ratio of the two streams.

Penetration of the perpendicular jets behind the steps in the supersonic flow was investigated experimentally by Yamauchi *et al.* [**5**] to understand the effects of the merging of the recirculation at the step base and ahead of the jets. It was observed that the slope of the Mach disc height plotted versus the dynamic pressure ratio reduced as the merger occurs and the merging improved the lateral spread of the injectant near the injector, thus improving ignition characteristics.

Gruber and Gross [**6**] experimentally studied the performance of gaseous injection for circular and elliptical orifices into supersonic cross-flow for different jet-to-free stream momentum ratio. The wall static pressures around the two orifices are measured using pressure sensitive paints.

Mixing characteristics of normal injection into a supersonic backward-facing step flow were investigated experimentally by Kuratani *et al.* [**7**] and Ikeda *et al.* [**8**]. The average and RMS velocity profiles and vorticity distribution in the compressible mixing layer between the normal injected flow and the inlet airflow were measured using particle image velocimetry (PIV) technique to find out the behaviour of the recirculation zone and the height of the Mach discs. Although these studies have explained important flow features of normal injection behind backward-facing step, the test section height was kept sufficiently high and the effect of confinement on the flow structure was not studied. In the practical scramjet combustor, for volume limited application, the height of the combustor is sufficiently less and confinement plays an important role in the flow development.

McDaniel *et al.* [**9**, **10**] studied experimentally the cold flow mixing of transverse sonic jets in a supersonic flow in a confined environment. A staged injection of sonic transverse jet is considered behind a backward-facing step in a Mach 2 stream. Detailed flow visualization and extensive measurements of various flow parameters at different cross-sections presented in the study can be very useful to validate any CFD software. Detailed measurements of the mole fraction of this experimental condition were carried out by Abbitt *et al.* [**11**] to study the evolution of supersonic mixing in the combustor.

Various numerical simulations of transverse sonic jet injections into supersonic cross-flows have been described in recent literature. Two-dimensional mixing flow calculations [**12**–**14**] showed results that qualitatively predicted the whole flow pattern. However, the quantitative prediction of the separated region was not so encouraging. Three-dimensional Navier–Stokes simulations [**15**, **16**] were also attempted to study the transverse injection flow with Baldwin–Lomax turbulence model. The comparisons of the computed flow parameters with experimental results show a reasonably good agreement. Uenishi *et al.* [**15**] carried out three-dimensional Navier–Stokes calculations with Baldwin – Lomax turbulence model for transverse sonic injection in a supersonic flow in a constant area combustor using MacCormack's explicit method and obtained qualitative agreement with the experimental results. Sun *et al.* [**17**] have carried out two- and three-dimensional Navier–Stokes simulation of supersonic turbulent flow field with transverse

sonic injection through a flat plate using weighted essentially non-oscillating (WENO) scheme and Jone–Launder K–ε turbulence model. Although computed surface pressures match well with the experimental value [**18**] for two-dimensional case, no comparisons with the experimental results are presented for three-dimensional case.

Lee and Mitani [**19**] have studied the comparative performance of the three transverse injectors for mixing augmentation in scramjet combustor using a three-dimensional Navier–Stokes equation along with K–ω SST model. Edward's low diffusion flux-splitting upwind difference scheme was used for discretization. It has been observed that the mixing characteristics are strongly related to jet-to-cross-flow momentum ratio. In case of higher values of momentum ratio, slower mixing rates, higher penetration, and more losses of stagnation pressure are shown.

Hao and Yu [**20**] have conducted numerical simulation of the flow field created by sonic transverse injection through a circular nozzle into a supersonic flow. Three-dimensional equations are solved using extended conservation element and solution element (CESE) method and the injectant penetrations are computed. Qualitative features of vorticity and injectant concentration at various cross-sections of the flow field have been presented. Backward-facing step and staged injection are generally employed in the scramjet combustor to avoid intake combustor interaction. Numerical simulation of sonic transverse injection in a supersonic flow in a confined environment has not been reported adequately in the literature.

Chakraborty *et al.* [**21**] carried out numerical exploration of staged transverse sonic injection behind backward-facing steps in a confined environment using three-dimensional Navier–Stokes equations that use Cartesian grid along with K–ε turbulence model with wall functions and obtained reasonable agreement with the experimental value of injectant penetration and various flow profiles at various axial locations of the combustor. As accurate prediction of wall heat transfer and skin friction are very important for the performance of scramjet combustor and these wall properties cannot be predicted accurately with Cartesian grid, numerical simulation are carried out in the present work with body-fitted coordinate. Experimental conditions of McDaniel *et al.* [**9**, **10**] are simulated numerically employing three-dimensional Navier–Stokes solver with K–ε turbulence model using a commercial CFD software CFX-TASCFlow [**22**]. The computed injectant penetration profiles and various flow parameters are compared with the experimental values and the other computational results.

2 METHODOLOGY

The software used in the present study is a three-dimensional Navier–Stokes code, CFX-TASCFlow [**22**], which is an integrated software system capable of solving diverse and complex multidimensional fluid flow problems. The code is fully implicit, finite volume method with finite element-based discretization of geometry. The method used retains much of the geometric flexibility of finite element methods as well as the important conservation properties of the finite volume method. It utilizes numerical upwind schemes to ensure global convergence of mass, momentum, energy, and species. It implements a general, non-orthogonal, structured, boundary-fitted grids. In the present study, the discretization of the convective terms are done by first-order upwind difference scheme. The turbulence model used was K–ε model with wall functions.

2.1 Governing equations

The appropriate system of equations, which governs the turbulent flow of a compressible gas, may be written as:

(a) continuity equation

$$\frac{\partial \rho}{\partial t} + \frac{\partial}{\partial x_k}(\rho u_k) = 0, \quad k = 1, 2, 3$$

(b) momentum equation

$$\frac{\partial}{\partial t}(\rho u_i) + \frac{\partial}{\partial x_k}(\rho u_i u_k) + \frac{\partial P}{\partial x_i} = \frac{\partial(\tau_{ik})}{\partial x_k},$$

$$i, k = 1, 2, 3$$

(c) energy equation

$$\frac{\partial}{\partial t}(\rho H) + \frac{\partial}{\partial x_k}(\rho u_k H) = -\frac{\partial}{\partial x_k}(u_j \tau_{jk}) + \frac{\partial q_k}{\partial x_k},$$

$$j, k = 1, 2, 3$$

(d) turbulent kinetic energy (K) equation

$$\frac{\partial}{\partial t}(\rho K) + \frac{\partial}{\partial x_k}(\rho u_k K) = \frac{\partial}{\partial x_k}\left(\left(\frac{\mu_l}{\mathrm{Pr}} + \frac{\mu_t}{\sigma_K}\right)\frac{\partial K}{\partial x_k}\right) + S_K$$

(e) rate of dissipation of turbulent kinetic energy (ε) equation

$$\frac{\partial}{\partial t}(\rho \varepsilon) + \frac{\partial}{\partial x_k}(\rho u_k \varepsilon) = \frac{\partial}{\partial x_k}\left(\left(\frac{\mu_l}{\mathrm{Pr}} + \frac{\mu_t}{\sigma_\varepsilon}\right)\frac{\partial \varepsilon}{\partial x_k}\right) + S_\varepsilon$$

(f) species mass fraction (Z)

$$\frac{\partial}{\partial t}(\rho Z) + \frac{\partial}{\partial x_k}(\rho u_k Z) = \frac{\partial}{\partial x_k}\left(\left(\frac{\mu_l}{\mathrm{Pr}} + \frac{\mu_t}{\sigma_c}\right)\frac{\partial Z}{\partial x_k}\right)$$

where ρ, u_i, p, and H are the density, velocity components, pressure, and total energy, respectively and $\mu = \mu_l + \mu_t$ is the total viscosity; μ_l, μ_t being the laminar and turbulent viscosity and Pr is the Prandtl number. The source terms S_K and S_ε of the K and ε equation are defined as

$$S_K = \tau_{ik}\frac{\partial u_i}{\partial x_k} - \rho\varepsilon \quad \text{and}$$

$$S_\varepsilon = C_{\varepsilon 1}\tau_{ik}\frac{\partial u_i}{\partial x_k} - C_{\varepsilon 2}\frac{\rho\varepsilon^2}{K}$$

where turbulent shear stress is defined as

$$\tau_{ik} = \mu_t\left(\frac{\partial u_i}{\partial x_k} + \frac{\partial u_k}{\partial x_i}\right)$$

Laminar viscosity (μ_l) is calculated from Sutherland law as

$$\mu_l = \mu_{ref}\left(\frac{T}{T_{ref}}\right)^{3/2}\left(\frac{T_{ref}+S}{T+S}\right)$$

where T is the temperature and μ_{ref}, T_{ref}, and S are known coefficients. The turbulent viscosity (μ_t) is calculated as

$$\mu_t = c_\mu\frac{\rho K^2}{\varepsilon}$$

The coefficients involved in the calculation of μ_t are taken as: $c_\mu = 0.09$, $C_{\varepsilon 1} = 1.44$, $C_{\varepsilon 2} = 1.92$, $\sigma_K = 1.0$, $\sigma_\varepsilon = 1.3$, and $\sigma_c = 0.9$. The heat flux (q_k) is calculated as $q_k = -\lambda(\partial T/\partial x_k)$; λ is the thermal conductivity.

2.2 Discretization of governing equations

The CFX-TASCFlow solver utilizes a finite volume approach, in which the conservation equations in differential form are integrated over a control volume described around a node, to obtain an integral equation. The pressure integral terms in the momentum integral equation and the spatial derivative terms in the integral equations are evaluated using finite element approach. An element is described with eight neighbouring nodes. The advective term is evaluated using upwind differencing with physical advection correction. The set of discretized equations form a set of algebraic equations: $\mathbf{A}\,\boldsymbol{x} = b$, where $\boldsymbol{x}$ is the solution vector. The solver uses an iterative procedure to update an approximated x_n (solution of x at nth time level) by solving for an approximate correction x' from the equation $\mathbf{A}\,\boldsymbol{x}' = \boldsymbol{R}$, where $\boldsymbol{R} = \boldsymbol{b} - \mathbf{A}\,\boldsymbol{x}_n$ is the residual at nth time level. The equation $\mathbf{A}\ \boldsymbol{x}' = \boldsymbol{R}$ is solved approximately using an approach called incomplete lower upper factorization method. An algebraic multigrid method is implemented to reduce low frequency errors in the solution of the algebraic equations. Maximum residual $(=\phi_j^{n+1} - f(\phi_j^{n+1}, \phi_j^n)) < 10^{-4}$ is taken as convergence criteria.

3 RESULTS AND DISCUSSIONS

The test cases for which numerical solutions are presented here are taken from the experimental study of McDaniel *et al.* [**9**, **10**]. Two sets of experiments were conducted by McDaniel *et al.* to study the cold flow mixing of staged transverse sonic injection into a Mach 2 flow behind a backward-facing step. In the first experiment [**9**], the injectant penetration and spreading profiles are presented for three different pressure ratios of the injectant and free stream static pressures, whereas the detailed measurements of various flow parameter profiles at various axial locations of the combustor are described in the second experiment [**10**]. The schematic of the grid distribution in the injection plane along with the boundary conditions in computational domain is presented in Fig. 2. The details of the combustor geometry are presented in Table 1. There are marginal differences between the two cases for the test section length (L), height (H), width (W), step height (h), the injector diameter (D), and the injector location; only the step locations for these two geometries differ. The primary purpose of the step is to isolate the inlet boundary layer from the pressure rise generated in the combustor. The step and the fuel injector staging are also expected to improve the penetration and mixing of fuel with the oxidizer and to create a recirculation region, which are important to sustaining the combustion.

In case 1 [**9**], injection penetration and spreading are measured from the laser-induced iodine fluorescence (LIIF) photographs for three different values of dynamic pressure ratios (Q) defined as

$$Q = \frac{1}{M_\alpha^2}\frac{P_{in}}{P_\alpha}$$

where, P_{in} is the injectant pressure and P_α and M_α are the main air steam static pressure and Mach number, respectively. The value of free stream pressure is 35.5 kPa and the injectant static pressure varied from 53.24 to 155.2 kPa giving values of Q from 0.35 to 1.02. In case 2 [**10**], only one condition is simulated with injectant pressure and air stream pressure of 263.0 and 274.0 kPa, respectively. The inflow parameters used in the simulations are summarized in Table 2.

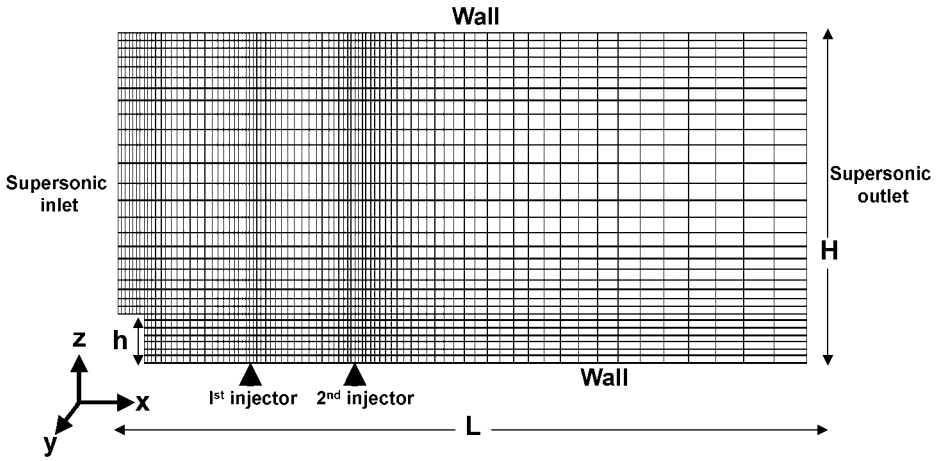

Fig. 2 Grid distribution in the computational domain

Table 1 Geometrical details of the combustor

Geometrical parameters	Case 1 [**9**] (mm)	Case 2 [**10**] (mm)
Test section length (L)	83.18	71.85
Test section height (H)	21.275	21.290
Test section width (W)	29.200	30.48
Step height (h)	3.175	3.218
Injector diameter (D)	2.0	1.93
Step location	−12.7	−9.534
1st injector location	0.0	0.0
2nd injector location	12.7	12.7

3.1 Injectant penetration and spreading

To study the injectant penetration and spreading, McDaniel and Graves [**9**] used a Mach 2.07 flow in a confined three-dimensional duct with length, height, and width of 83.18, 18.1, and 21.275 mm, respectively. The details of geometry and the inflow parameters are presented in Tables 1 and 2, respectively.

In the simulation, the x axis is taken along the length of the combustor and y and z axes are taken along the width and the height of the combustor, respectively. The centre of the first injector at the injection plane ($z = 0$) is taken as the origin. The inflow and outflow boundaries are placed at 16 mm ($8D$) upstream and 67.3 mm ($33.65D$) downstream of the first injection point. A non-uniform grid of size $81 \times 41 \times 31$ is used in the simulation. The grids are fine near the step, injector locations, and near-wall region and relatively coarse in the rest of the field. The grid independence of the results is demonstrated by comparing the pressure profile at the injector plane of the 1st injector location ($x/D = 0$, $y/D = 0$) with three different grids, namely, $69 \times 29 \times 24$, $81 \times 41 \times 31$, and $92 \times 49 \times 35$ in Fig. 3. It is clear from the figure that by changing the grid from $81 \times 41 \times 51$ to $92 \times 49 \times 35$, the results almost remain unchanged, thus presenting the grid independence of the results. The qualitative

Table 2 Inflow parameters for the computation

	Case 1		Case 2	
Parameter	Air stream	Injector	Air stream	Injector
Free stream total pressure (P_o), kPa	310.0	101.0 204.4 294.0	274.0	263.0
Free stream static pressure (P_α), kPa	35.53	53.24 108.0 155.2	35.0	139.0
Mach number (M)	2.07	1.0	2.0	1.0
Dynamic pressure ratio of air stream and injectors (Q)		0.35 0.71 1.02		0.993
Free stream total temperature (T_o), K	298.1	298.1	300.0	300.0
Free stream static temperature (T_α), K	160.5	248.4	167.0	250.0
Free stream velocity (u_α), m/s	527.2	316.5	518.0	317.2
Molecular weight	28.8	28.86	28.8	28.86
Specific heat ratio (γ)	1.4	1.4	1.4	1.4

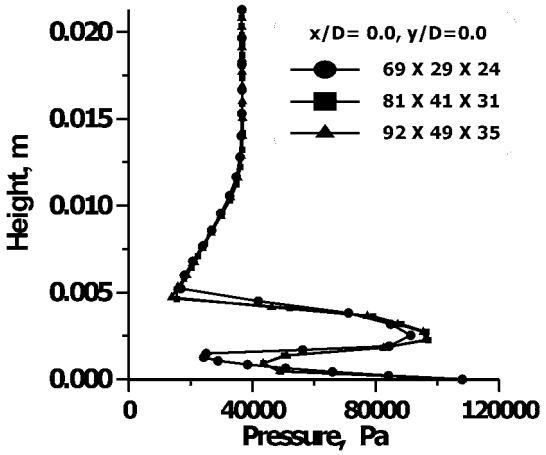

Fig. 3 Pressure profile variation with different grids

features of the flow field are presented through the velocity vector plot in the plane of injection ($y/D = 0$) in Fig. 4; the streak lines of the flow field are also plotted in the figure. The bow shock ahead of the injection and the two barrel shocks are clearly visible. The low-speed recirculation zones are formed behind the backward-facing step and the region between the two injections. The injection mass fraction distribution at the injection plane is presented in Fig. 5. The injectant could not penetrate into the upper wall even at the exit of the combustor. Injectant mass is also seen in the recirculating zone near the backward-facing step.

The computed injectant penetration profiles are compared with the experimental data [**9**] and the result of the other numerical computation [**21**] for three values of Q (= 0.35, 0.71, and 1.02) in the injection plane ($y/D = 0$) in Fig. 6. The injectant penetration is compared in terms of the distance along the height where the mole fraction of the injectant is 1 per cent (as was done in the experiment). A good overall match between the computation and experiment is observed. As expected with the increase of the dynamic pressure ratio, the penetration of the injectant is increased. The present computation predicts the injection penetration profile better, compared with the PARAS3D simulation [**21**], particularly in the zone near the orifice in spite of using 0.16 million grids in comparison with 0.68 million grids [**21**]. This is due to the fact that the final adopted grid in PARAS3D [**21**] is not optimal. If any parameter is having a gradient in one direction, the adopted grid-splitting methodology [**21**] splits the mother cell in three directions making eight child cells, introducing additional grids in other direction. The spreading of the injectant (1 per cent mole fraction at the $1.0D$ distance above the injection plane) for three dynamic pressure ratios is compared with the experimental values in Fig. 7. A reasonably good match between the computed and experimental values is obtained. It has been observed that dynamic pressure does not affect the spreading significantly.

3.2 Comparison of the flow-field parameters

Detailed flow-field measurements in the combustor are given in reference [**10**]. The experimental conditions (i.e. combustor geometry and inflow parameters) for this case are slightly different than for

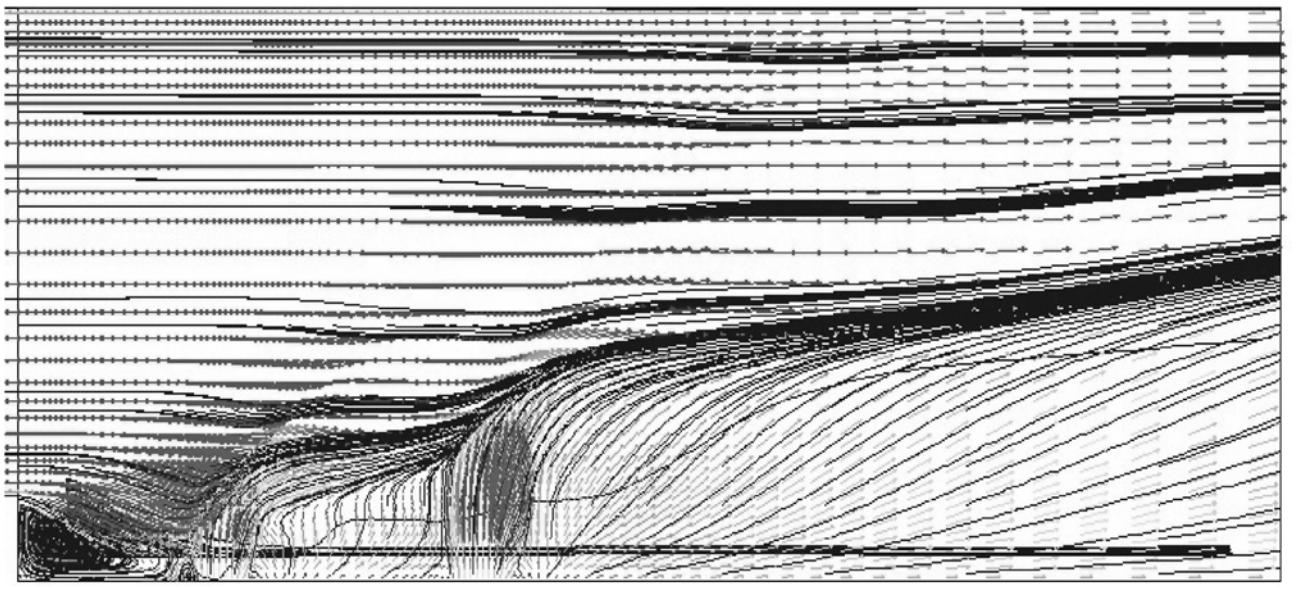

Fig. 4 Velocity vector with streak line plot ($y/D = 0.0$)

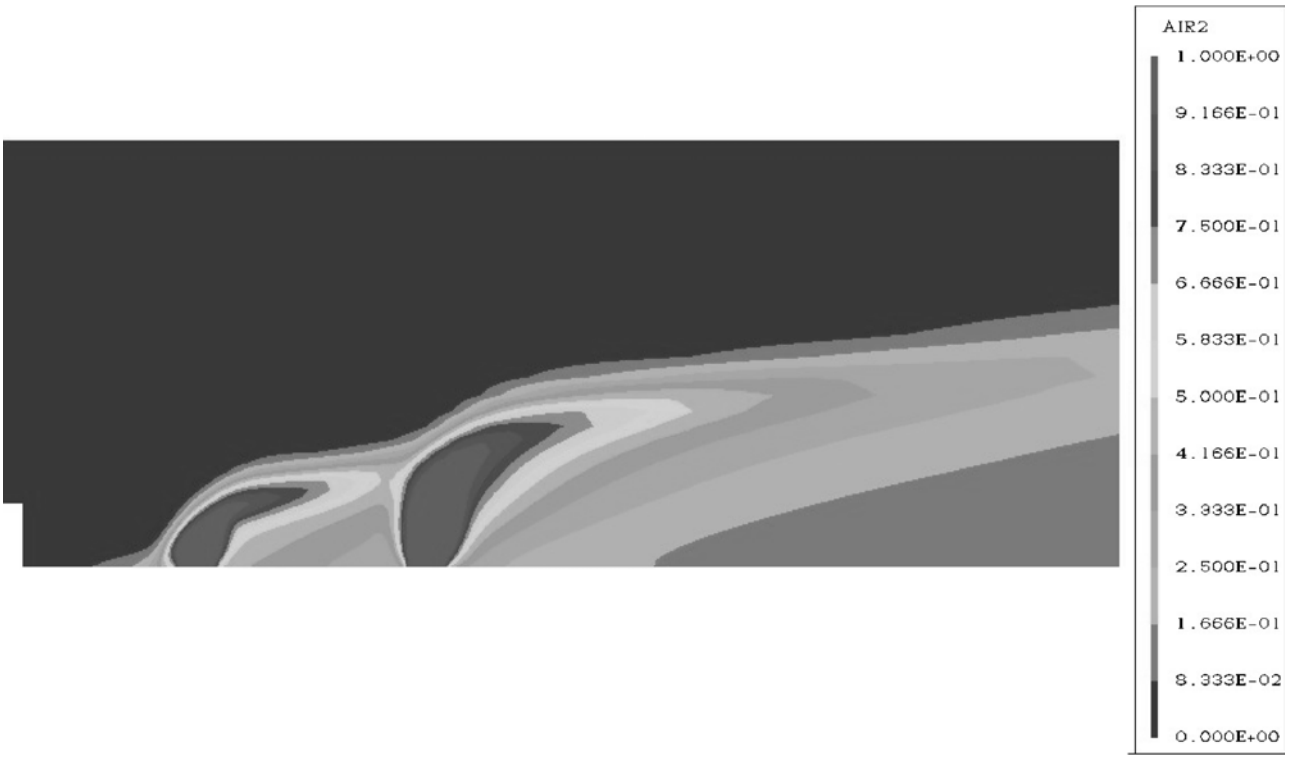

Fig. 5 Injectant mass fraction distribution ($y/D = 0.0$)

the first case as explained earlier. A new numerical simulation is carried out for this combustor geometry. The non-dimensionalized pressure (P/P_α) profile at $x/D = 0$ is compared with the experimental data [**10**] and other computational results [**21**] in Fig. 8(a). At $x/D = 0$, in the far-field region of orifice ($z/D > 2.0$), the comparison is satisfactory, but in the near-flow region ($z/D < 2.0$), although the trend is matched, the magnitude differs considerably. In the near-field zone, even the two experimental results (PLIIF and LIIF) show a difference of more than 30 per cent, indicating a complex flow structure near the injection orifice. The comparison of the pressure profile at $x/D = 3.0$ (Fig. 8(b)) (located between the two injectors) is reasonable. Similar conclusion can be drawn from the comparison of the pressure profiles at $x/D = 6.6$ (at the second injection orifice) and $x/D = 12.8$ (downstream location) represented in Figs 8(c) and (d), respectively. Possible reasons for the difference of the results near the injection orifices may be conjectured as follows.

1. In the computation, a uniform injection flow field corresponding to the sonic Mach number at the injection orifice zone is considered, but the measured value of the Mach number of the exit plane of the orifice [**10**] shows a non-uniform profile. The mean value of the injector exit Mach number shows a value of ~1.5 near the upstream and downstream edges and ~1.0 at the centre-line

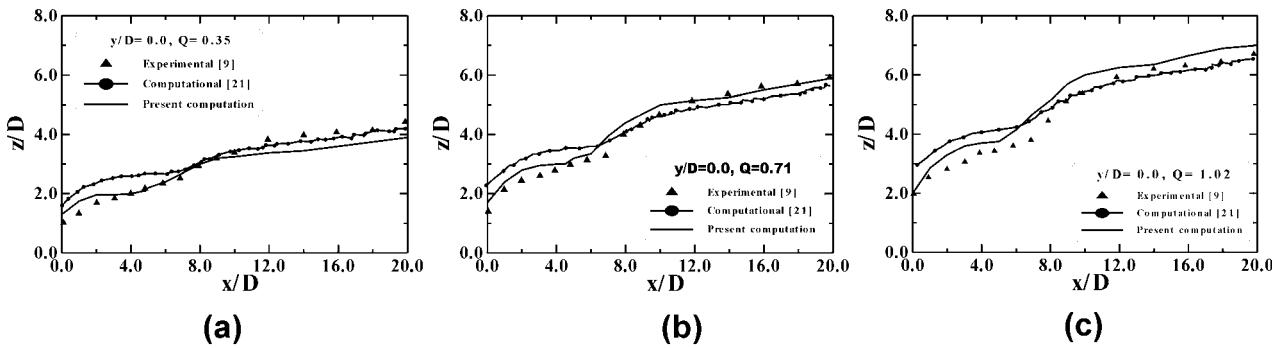

Fig. 6 Comparison of injectant penetration: (a) $Q = 0.35$, (b) $Q = 0.71$, and (c) $Q = 1.02$

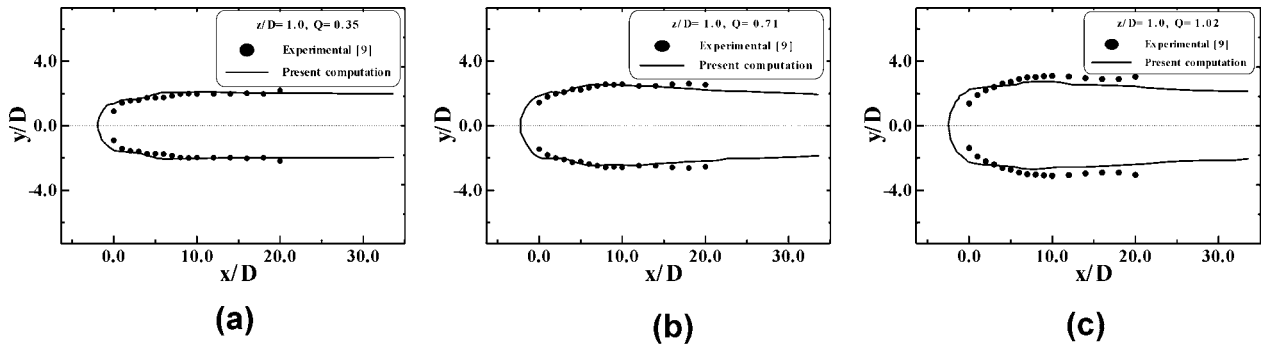

Fig. 7 Comparison of injectant spreading: (a) $Q = 0.35$, (b) $Q = 0.71$, and (c) $Q = 1.02$

of the orifice. The simulation with this non-uniform profile is yet to be undertaken.

2. The inadequacy of the eddy viscosity turbulence model to predict the flow field in a zone where distinct scales exist.

The computed axial velocity profiles at $x/D = 0$, 3.0, 6.6, and 12.8 are compared with the experimental results and the other computational results of Figs 9(a) to (d), respectively. A good agreement among the experimental results, other computational results, and the present computations has been obtained for all the four axial locations. Finally, the velocity profiles in the z-direction at $x/D = 0$, 3.0, 6.6, and 12.8 are compared in Figs 10(a) to (d), respectively, which show a good agreement between experimental and present computational values.

4 CONCLUSIONS

The capability of the software CFX-TASCFlow for non-reacting turbulent supersonic flow analysis is demonstrated. The experimental conditions of

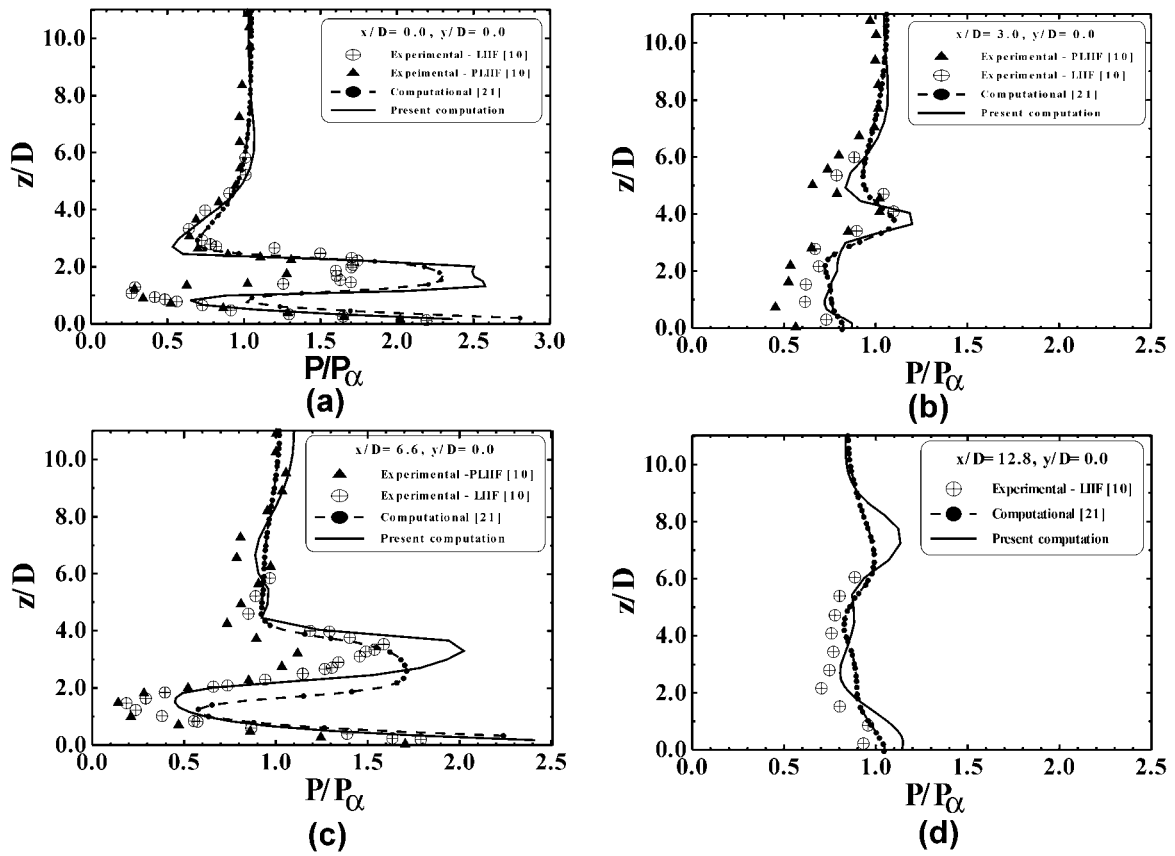

Fig. 8 Comparison of pressure distribution: (a) $x/D = 0.0$, (b) $x/D = 3.0$, (c) $x/D = 6.6$, and (d) $x/D = 12.8$

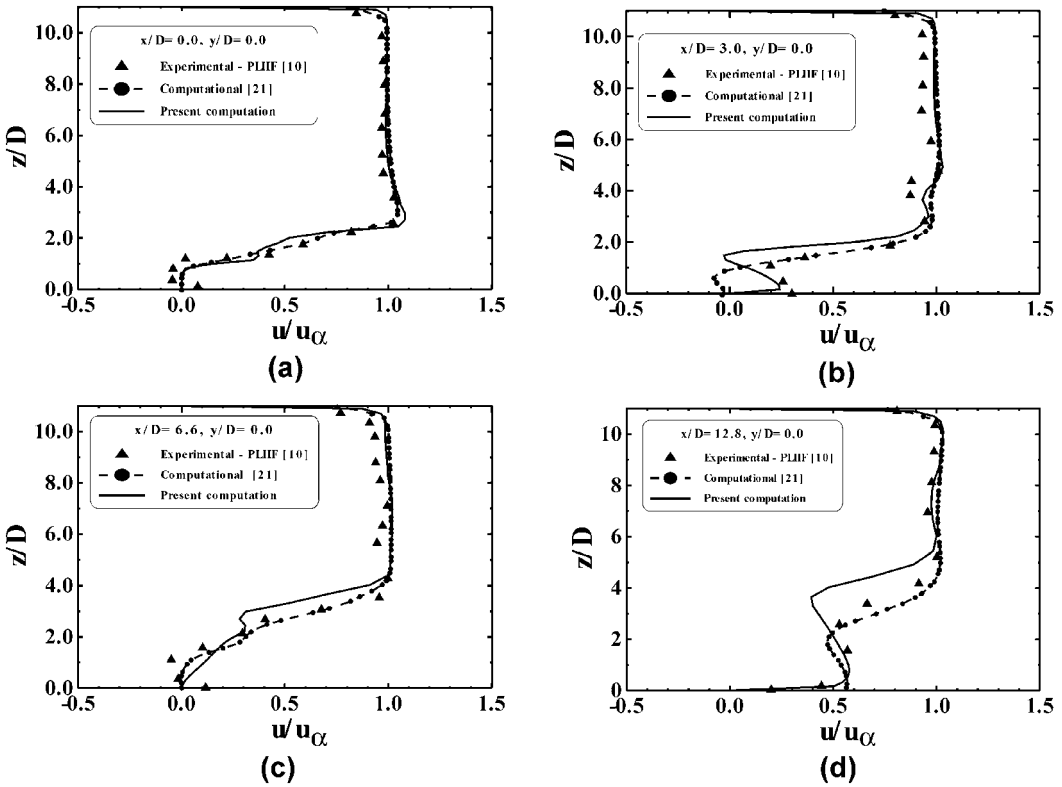

Fig. 9 Comparison of velocity (u) profile: (a) $x/D = 0.0$, (b) $x/D = 3.0$, (c) $x/D = 6.6$, and (d) $x/D = 12.8$

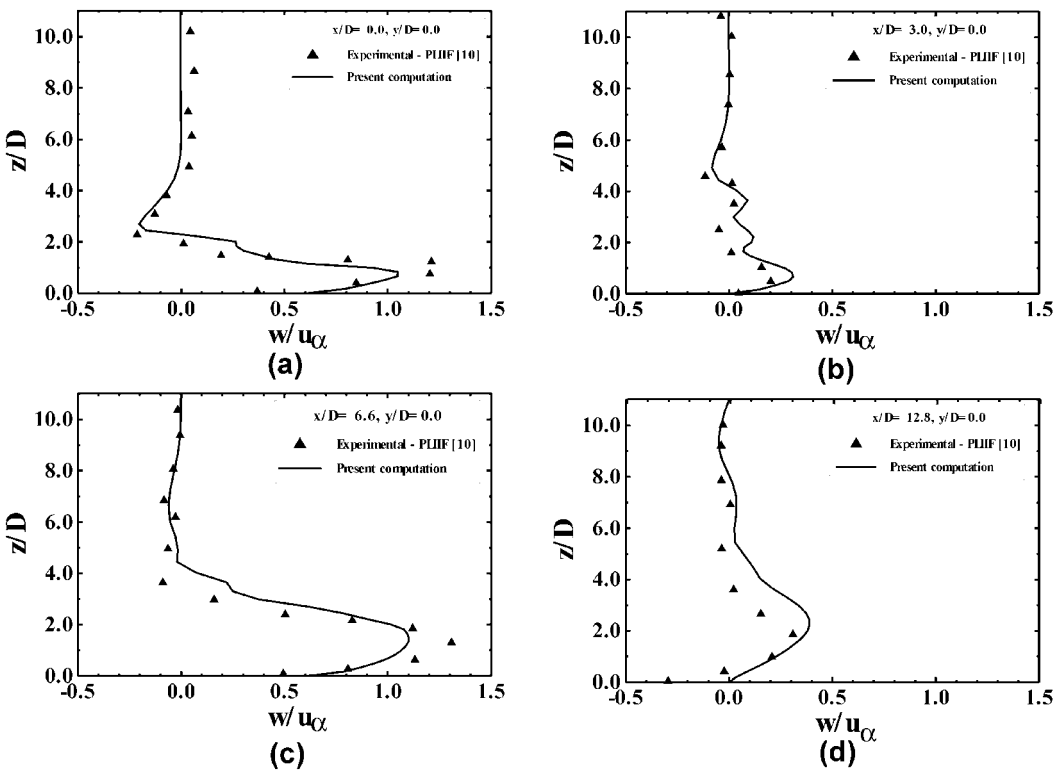

Fig. 10 Comparison of velocity (w) profile: (a) $x/D = 0.0$, (b) $x/D = 3.0$, (c) $x/D = 6.6$, and (d) $x/D = 12.8$

McDaniel *et al.* [**9**, **10**] are considered as validation cases for studying the mixing characteristics of sonic air injections in supersonic streams behind a backward-facing step. Three-dimensional Navier–Stokes equations are solved along with K–ε turbulence model. A good agreement is obtained for the injectant penetration and spreading between the present computation and the experimental and other computational [**21**] results. It has been observed that the dynamic pressure ratio does not affect the spreading significantly. The present computation predicts reasonably well the flow-field parameters in the zone away from the injection region, whereas there are differences in the value in the near-field region. The difference could be due to the assumption of uniform flow at the injection orifice and/or inadequacy of the K–ε turbulence model to predict the flow field where the distinct scales exist.

REFERENCES

1 **Zukoski, E. E.** and **Spaid, F. W.** Secondary injection of gases into a supersonic flow. *AIAA J.*, 1964, **2**(10), 1689–1696.

2 **Schetz, J. A., Hawkins, P. F.,** and **Lehman, H.** Structure of highly underexpanded transverse jets in a supersonic stream. *AIAA J.*, 1967, **5**(5), 882–884.

3 **Hersch, M., Povinelli, L. A.,** and **Povinelli, F. P.** Optical study of sonic and supersonic jet penetration from a flat plate into a Mach 2 airstream. *NASA TN D-5717*, 1970.

4 **Papamoschou, D., Hubbard, D. G.,** and **Lin, M.** Observations of supersonic transverse jets. AIAA paper 91-1723, 1991.

5 **Yamauchi, K., Kitadani, H., Masuya, G., Tomioka, S.,** and **Izumikawa, M.** Penetration of jets injected behind backward-facing step in supersonic stream. AIAA paper 99-2106, 1999.

6 **Gruber, M. R.** and **Gross, L. P.** Surface pressure measurements in supersonic transverse injection flowfields. *J. Propuls. Power*, 1999, **15**(5), 633–641.

7 **Kuratani, N., Ikeda, Y., Nakajima, T., Tomioka, S.,** and **Mitani, T.** Mixing characteristics of normal injection into a supersonic backward facing step flow measured with PIV. AIAA paper 2002-0237, 2002.

8 **Ikeda, Y., Kuratani, N., Nakajima, T., Tomioka, S.,** and **Mitani, T.** M2.5 supersonic PIV measurement in step-back flow with the normal injection. AIAA paper 2002-0232, 2002.

9 **McDaniel, J. C.** and **Graves, J., Jr.** Laser-induced-fluorescence visualization of transverse gaseous injection in a nonreacting supersonic combustor. *J. Propul. Power*, 1988, **4**(6), 591–597.

10 **McDaniel, J. C., Fletcher, D. G., Hartfield, R. J.,** and **Hollo, S. D.** Staged transverse injection into Mach 2 flow behind a rearward facing step: a 3-D compressible test case for hypersonic combustor CFD validation. AIAA paper 92-0827, 1992.

11 **Abbitt, J. D., III, Hartfield, R. J.,** and **McDaniel, J. C.** Mole-fraction imaging of transverse injection in a ducted supersonic flow. *AIAA J.*, 1991, **29**(3), 431–435.

12 **Weinder, E. H.** and **Drummond, J. P.** Numerical study of staged fuel injection for supersonic combustion. *AIAA J.*, 1982, **20**(10), 1426–1431.

13 **Rizzeta, D. P.** Numerical investigation of slot jet injection into a turbulent supersonic stream. AIAA paper 92-0839, 1992.

14 **Clark, S. W.** and **Chan, S. C.** Numerical investigation of a transverse jet for supersonic aerodynamic control. AIAA paper 92-0639, 1992.

15 **Uenishi, K., Rogers, R. C.,** and **Northam G. B.** Numerical predictions of a rearward-facing-step flow in a supersonic combustor. *J. Propul. Power*, 1989, **5**(2), 158–164.

16 **Lee, J.** Numerical study of mixing in supersonic combustors with hypermixing injectors. *J. Propul. Power*, 1994, **10**(3), 297–304.

17 **Sun, D., Amano, R. S.,** and **Cai, T.** Simulation of supersonic turbulent flowfield with transverse sonic injection. AIAA paper 2002-0162, 2002.

18 **Aso, S.** and **Okuyama, S.** Experimental study on mixing phenomena in supersonic flow with slot injection. AIAA paper 91-0016, 1991.

19 **Lee, S. H.** and **Mitani, T.** Mixing augmentation of transverse injection in scramjet combustor. *J. Propul. Power*, 2003, **19**(1), 115–124.

20 **Hao, H.** and **Yu, S. T. J.** Three-dimensional simulation of transverse injection in a supersonic flow by the CESE method. AIAA paper 2003-0375, 2003.

21 **Chakraborty, D., Roychowdhury, A. P., Ashok, V.,** and **Kumar, P.** Numerical investigation of staged transverse sonic injection in Mach 2 stream in confined environment. *Aeronaut. J.*, 2003, **107**(1078), 719–729.

22 *CFX-TASCFlow Computational Fluid Dynamics Software, Version 2.11.1*, 2001 (AEA Technology Engineering Software Ltd).

APPENDIX

Notation

A	coefficient matrix
D	diameter of the injectors
h	step height
H	enthalpy, also height of the combustor
K	turbulent kinetic energy
L	length of the combustor
M	Mach number
P	pressure
Pr	Prandtl number
q	heat flux
Q	dynamic pressure ratio
R	residue
S	Sutherland constant
S_K, S_ε	source terms for K and ε

t	time
T	temperature
u	velocity
x, y, z	coordinate axes
Z	species mass fraction
W	width of the combustor
ρ	density
τ	shear stress
ε	turbulent kinetic energy dissipation rate
μ	dynamic viscosity
σ_K, σ_ε, σ_c	coefficients for K, ε, and Z equations
λ	thermal conductivity
γ	ratio of specific heats

Subscripts

i, j, k	axial direction
in	injectant
l	laminar
o	stagnation value
ref	reference value
t	turbulent
α	free stream static value